Photonic Crystal Slab Waveguides Based on Antiresonant Reflecting Optical Waveguide Structures

Yu-Lin Yang, Shih-Hsin Hsu, *Member, IEEE*, Ming-Feng Lu, and Yang-Tung Huang, *Member, IEEE*

***Abstract*—A novel two-dimensional photonic crystal slab waveguide based on an antiresonant reflecting optical waveguide (ARROW) structure is proposed and designed. Lightwaves propagating in this waveguide are confined by antiresonance reflection vertically and the photonic band gap laterally. In order to obtain the characteristics of the ARROW-based photonic crystal waveguides, the three-dimensional finite-difference time-domain simulations are performed. With a lateral adiabatic taper, a coupling efficiency of 80.3% from a single-mode fiber to the ARROW-based photonic crystal waveguide of a single-line defect is obtained. In addition, propagation losses less than 10 dB/mm and bend losses of 0.23 and 0.39 dB/bend for the designed 60° and 120° bends are achieved at an operating wavelength of 1.55 μm.**

***Index Terms*—Antiresonant reflecting optical waveguide (ARROW), bending waveguide, finite-difference time-domain (FDTD) method, photonic crystals (PCs), propagation loss.**

I. Introduction

TWO-DIMENSIONAL (2-D) photonic crystal (PC) waveguides have the strong potential for constructing ultra-compact photonic integrated circuits due to their abilities of controlling lightwaves. In general, the waveguides are formed by introducing line defects into the lattices of air holes in dielectric slabs. Lightwaves are confined in-plane by the photonic band gap, in which propagation of photons is forbidden. Utilizing this attractive advantage, waveguiding in straight channels [1]–[7] and even sharp bends [8]–[11] with low losses can be realized. In the vertical direction, there have been two types of guiding mechanisms demonstrated in the previous literatures. First, the 2-D PC slab waveguides of high-index-contrast type are implemented by means of suspending the thin core membrane in air [1] or patterning structures in silicon-on-insulator (SOI) wafers [2], [3] for providing strong confinement. However, the low propagation loss have been achieved only in the narrow bandwidth in this configuration. Second, the low-index-contrast PC slab waveguides are usually investigated in InP-based [4] or GaAs-based [5] heterostructures. Since the guided modes of PC waveguides exist above the light lines of cladding layers, severe vertical radiation losses exhibit in the single-line-defect waveguides [12]. To obtain high transmission, the multimode propagation is unavoidable.

In practical applications, it is desirable to connect PC waveguides with fibers. However, owing to the large impedance mismatch between them, finding an efficient and direct method for coupling lightwaves into and out off PC circuits is not a trifle. To solve this difficulty, many couplers have been proposed such as gratings, mirrors, and fiber tapers [13]–[15], etc. For the butt coupling, however, it is still important to reduce the coupling losses in the vertical direction.

Compared with these two guiding mechanisms in the vertical direction, a 2-D PC slab waveguide with a relatively thick core layer is proposed and designed to improve the butt-coupling efficiency with a fiber in this report. In the vertical direction, we adopt the Fabry–Pérot cavities as reflectors [16], [17] under the core layer of a PC waveguide instead of one cladding layer of a lower refractive index. Lightwaves propagating in the core layer meet total internal reflection at the air-core interface, and very high reflection from the set of interfaces of the cavities. This structure so-called an antiresonant reflecting optical waveguide (ARROW) can be designed to support low loss propagation in a core layer of a relatively large size according to flexible design rules. Laterally, the periodic arranged air holes are implemented in the ARROW structure to provide the photonic-band-gap confinement. In our investigation, characteristics of the butt-coupling loss between the ARROW-based PC waveguide and a single-mode fiber, the propagation loss of the straight waveguide and bend losses at the 60° and 120° sharp bends are studied. All these losses are calculated by the finite-difference time-domain (FDTD) method performed in the commercial software (FullWAVE by RSoft).

II. Design of Arrow-Based PC Waveguides

As shown in Fig. 1(a), the ARROW structure is a multilayer planar waveguide consisting of a thick core layer of refractive index n_c, and two cladding layers of a high refractive index n_h

Manuscript received July 30, 2008; revised November 27, 2008. Current version published July 01, 2009. This work was supported by the National Science Council of the Republic of China under Contract NSC92-2215-E-009-047.

Y.-L. Yang is with the Department of Electronics Engineering and Institute of Electronics, National Chiao Tung University, Hsinchu 30010, Taiwan (e-mail: ylyang.ee93g@nctu.edu.tw).

S.-H. Hsu is with the Research Center for Applied Sciences, Academia Sinica, Taipei 11529, Taiwan (e-mail: shhsu.ee85g@nctu.edu.tw).

M.-F. Lu is with the Department of Electronics Engineering and Institute of Electronics, National Chiao Tung University, Hsinchu 30010, Taiwan, and also with the Department of Electronics Engineering, Minghsin University of Science and Technology, Hsinfeng, Hsinchu 304, Taiwan (e-mail: mflu@must.edu.tw).

Y.-T. Huang is with the Department of Electronics Engineering and Institute of Electronics, and the Department of Biological Science and Technology, National Chiao Tung University, Hsinchu 30010, Taiwan (e-mail: huangyt@cc.nctu.edu.tw).

Color versions of one or more of the figures in this paper are available online at http://ieeexplore.ieee.org.

Digital Object Identifier 10.1109/JLT.2009.2014692

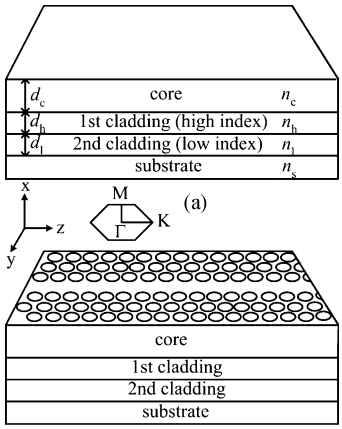

Fig. 1. Schematic pictures of (a) an ARROW structure and (b) an ARROW-based PC waveguide.

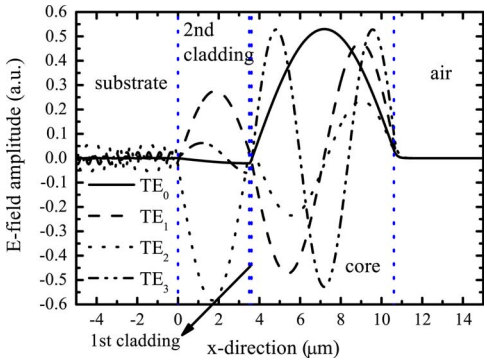

Fig. 2. Electric field profiles of the TE_0 to TE_3 modes for the planar ARROW structure.

TABLE I
EFFECTIVE INDICES AND THE PROPAGATION LOSSES OF TE AND TM MODES

	TE_0	TE_1	TE_2	TE_3	TM_0	TM_1
N_{eff} (real part)	1.998	1.991	1.990	1.981	1.997	1.989
loss (dB/cm)	0.02	25.48	105.18	1.13	1.17	326.60

and a low refractive index n_l between the core layer and substrate of index n_s. Lightwaves in the core layer are confined by means of total internal reflection at the air-core interface and ultrahigh reflection from the cladding layers. To attain a low insertion loss with a single-mode fiber, the thickness of the core layer d_c is chosen as 7.00 μm. The optimized and thinnest thicknesses of these two claddings d_h and d_l satisfy the antiresonance condition as [16]

$$d_h = \frac{\lambda}{4n_h}\left[1 - \frac{n_c^2}{n_h^2} + \left(\frac{\lambda}{2n_h d_c}\right)^2\right]^{-1/2} \quad (1)$$

$$d_l = \frac{d_c}{2} \quad (2)$$

where λ is the free-space operating wavelength and equal to 1.55 μm in our design. Many materials are transparent in the objective wavelength range and can be exploited in this structure. Here, we adopt the following parameters for the design: $n_c/n_h/n_l/n_s = 2.0/3.5/2.0/3.5$. The derived thicknesses of the first cladding d_h and the second cladding d_l are 0.13 and 3.50 μm, respectively. First, the modal characteristics of the planar ARROW structure are calculated by the transfer matrix method to obtain the effective index and the propagation loss for each transverse electric (TE) and transverse magnetic (TM) mode. For the TE_0 mode, the propagation loss is lower than that of higher order modes at least one order of magnitude, as listed in Table I. Reflections of TM modes from interfaces of claddings are always lower because of the existing of the Brewster angles. Therefore, the TM and higher order TE modes can be effectively filtered out due to the loss discrimination to maintain the quasi-single mode propagation. The electric field profiles for the planar ARROW structure are shown in Fig. 2. The quasi-guided TE_0 mode behaves like a fundamental guided mode in a conventional slab waveguide. The overlap integrals between the electric fields of the higher order modes and the TE_0 mode are all lower than 0.03%. This result indicates that the amounts of TE_0 mode converting into higher order modes are extremely small. In addition, the excitation coefficient of the TE_0 mode from the launched Gaussian profile is about 95.9%. Therefore, the losses from higher order modes can be neglected, and our discussion is focused on the TE_0 mode.

The PC pattern is embedded in the core layer of the ARROW structure. The periodicity of air holes is arranged with a triangular lattice structure, and a PC waveguide is formed by removing one row of air holes along the z-direction (Γ-K direction), as shown in Fig. 1(b). Air hole radius r is equal to $0.35a$, where a is one lattice constant. To probe the confinement of the PC waveguide in this guiding layer of a low refractive index ($n_c = 2.0$), the distribution of defect modes in the band diagram has to be confirmed. We convert the 3-D structure to an effective 2-D PC plane. The effective index of the TE_0 mode in the ARROW structure is used as the background index in the 2-D calculations, and the refractive index of air holes is still 1.0. By this approximation, the projected band structure is calculated with the 2-D plane-wave expansion (PWE) method and the supercell technique in the commercial software (BandSOLVE by RSoft), as shown in Fig. 3(a). It is found that two defect modes are induced in the range of the band gap, $0.370 \sim 0.450$ (a/λ). One is an even mode, and the other is an odd mode. The former's H_x field is symmetric to the bisecting plane of the PC waveguide, and the latter's is antisymmetric to that. The even mode existing from frequency 0.378 to 0.45 (a/λ) with a negative slope, stemming from the guided mode being folded at the edge of the Brillouin zone, is dominated by the index confinement. In the flat dispersion range from 0.370 to 0.378 (a/λ), it can be explained with the mechanism of the band gap confinement. In addition, the 2-D FDTD method with the effective index is used to compute related transmission spectra under the boundary condition of the perfectly matched layer (PML). The lattice constant a is specified as 0.66 μm and the spatial resolution is set as $a/20$ in the PC plane (yz-plane). A pulse with a Gaussian profile of TE mode is inputted in the front of the PC waveguide to mainly excite the even mode in the waveguide over a wide range of frequencies. The input power is set as unity. The time monitor is located at the end of the waveguide to detect the power transmission through it. By Fourier transforming the fields recorded

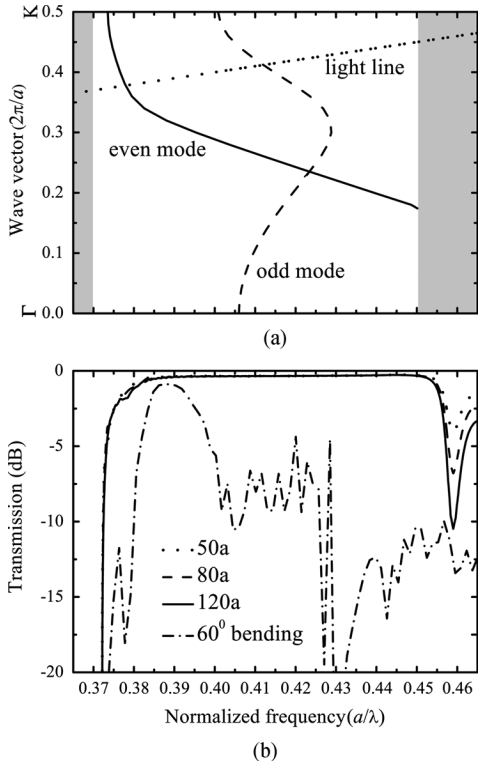

Fig. 3. (a) Projected TE band structure for the 2-D PC waveguide of the single-line defect. The light gray area is the region of PC bulk bands. (b) Related transmission spectra of the straight waveguides with different propagation lengths and the waveguide incorporated with a conventional 60° bend. The total propagation length of the bending waveguide is $20a$. These waveguides are all of nine rows of PCs on each side of guiding channels.

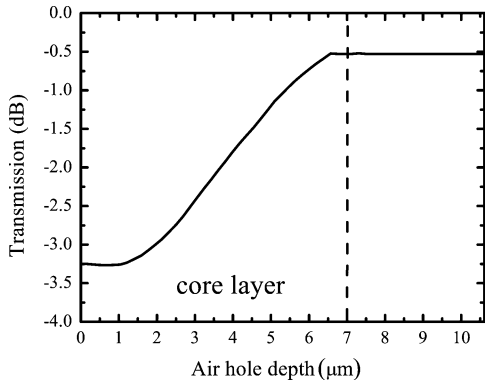

Fig. 4. Transmission versus air hole depth for the ARROW-based PC waveguide. The lattice constant a is 0.674 μm. The waveguide length is $20a$ with nine rows of PCs on each side of the guiding channel.

on the monitor in every time step, transmission spectra are calculated and shown in Fig. 3(b). It can be seen that the transmission spectra match well with the band structure except some blue shifts. In the frequency range of index guiding, transmission efficiencies can reach high values above 92%, and the propagation losses of the band-gap guided mode near the band edge are extremely low.

III. Butt-Coupling and Propagation Losses in ARROW-Based PC Waveguides

To obtain more accurate results, a fully 3-D calculation is necessary to compute the power radiate out of plane. The 3-D FDTD method and the boundary condition of PML are used for ARROW-based PC waveguides with grid sizes of $a/15$ in the yz-plane and 0.03 μm in the x-direction. Our devices are calculated with continuous waves at the wavelength of 1.55 μm as an input light source. The spatial distribution of the launched field is a Gaussian profile with a width of $\sqrt{3}a$ and a height of 7 μm. Without losing generality, the launched field is put in the center of the core layer. To verify the guiding mechanism of the ARROW-based PC waveguide, it is essential to find the relation between the transmission efficiency and the air hole depth. As shown in Fig. 4, the transmission reaches a saturation value as air hole depth is increased to 7.00 μm, which is the same as the thickness of the core layer. This is because the field of the TE_0 mode for an ARROW structure is mainly confined in the core layer, where the TE mode in the 3-D configuration is defined that the electric field is primarily along the y-direction. The air hole depth should be deep enough to enclose the tail of the mode sufficiently and confine the field laterally. As the depth of air holes is reduced, the field of lightwaves would penetrate into the PC bulk laterally to result in increase of propagation losses. The lightwaves becomes intrinsically radiative for the depth ≤ 1 μm, and the transmission still maintains around -3.3 dB due to the short propagation length in this simulation. Increasing the thickness of the core layer is beneficial for butt coupling with a single-mode fiber, whereas gives a challenge for the process of the deep etching. With the advanced integrated circuit technology, etching air holes of high aspect ratios has been achieved in previous papers [4], [18], [19]. This makes the ARROW-based PC waveguides realized more possibly.

For the SOI-type PC slab waveguides, the thickness of core layer is smaller than 0.3 μm to keep single-mode propagation. By simulating with the 3-D FDTD method, the butt coupling efficiency between the waveguide and the single-mode fiber, which has a core diameter 6 μm with a refractive index 1.451 and a cladding diameter 125 μm with an index 1.445, is shown as low as only 3.3% without the assistance of couplers. This efficiency can be significantly improved to 30.3% for the ARROW-based PC waveguide due to the relatively large core size and the matched refractive index of the core layer. There have been many lateral couplers proposed for efficiently converting guided modes from wide waveguides to narrow waveguides. Here, we consider the simplest case of an adiabatic taper, waveguide structure varing linearly along the propagation direction from the 7-μm width to the $\sqrt{3}a$ width, where a is equal to 0.674 μm. The single-mode fiber is directly butted in contact with the taper as shown in Fig. 5. Through this mode converter, it is found that the 95.1% of power from the fiber transmits through the interface between the fiber and the taper by the 3-D FDTD simulation. The taper itself conserves distribution of the power in the waveguide during propagation and provides a 89.1% transmission. In addition, the 3-D FDTD simulation gives a transmission of 94.8% through the interface of the taper and the ARROW-based PC waveguide. By means of multiplying these three values, the overall butt-coupling

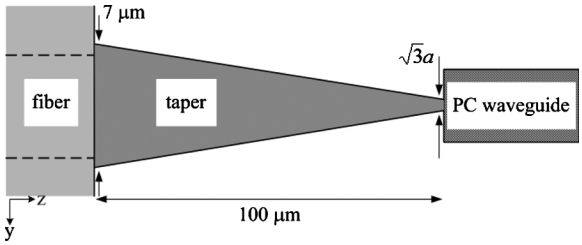

Fig. 5. Top view of the ARROW-based PC waveguide with an adiabatic taper connecting with the single-mode fiber.

efficiency of 80.3% is obtained between the fiber and the PC waveguide.

As discussed above, the light can be confined laterally by 2-D PCs based on the photonic band gap, and vertically in the core layer of the ARROW structure by satisfying the antiresonance condition. A propagation loss of a PC slab waveguide is an essential issue, however, performing its calculation is still difficult owing to large consumption of time and computational memories [12], [20], [21]. In this paper, the 3-D FDTD simulation is used for calculating the power of lightwaves transmission through the detecting monitors, which are placed along the waveguide of a length of $80a$. The distance between two adjacent monitors is fixed at three lattice constants. The propagation loss at each frequency can be obtained from the linear fit of the recorded transmission efficiencies on the monitors. The launched field is a Gaussian profile for exciting the even mode of PC in the band gap laterally and the TE_0 mode of ARROW structure vertically. The operating wavelength is fixed as 1.55 μm to keep the optimized performance of the ARROW structure, and the lattice constant a of the PC is varied to obtain the transmission spectrum, as shown in Fig. 6. In comparison with Fig. 3, the transmission spectrum of the ARROW-based PC waveguide agrees with the 2-D case and its corresponding projected TE band structure. Further, it can be seen that the losses gradually decrease from low to high frequencies, which is unobvious in transmission spectra of 2-D case. This can be simply explained that a mode of higher frequency is more refractive-like, and its field profile is well confined in the channel of the PC waveguide as shown in Fig. 7(a) and (b). Consequently, this causes less interaction between lightwaves and air holes [12], [21], resulting in less coupling to radiation modes in light cone of air. It is noticeable that the attenuation less than 10 dB/mm predicted for the ARROW-based PC waveguide is of the same order of magnitude for the PC slab waveguides of low-index-contrast type with a three-line defect [4]. In addition, PC waveguides on an ARROW platform still maintain single-mode propagation both in the vertical and the lateral directions. Lightwaves of the TE_0 mode propagating in the core layer of the ARROW structure with larger ray angles results in the less number of reflection at the air-core interface. Even operating in the radiation region (above the light line), therefore, the ARROW-based PC waveguides can keep acceptable losses for the photonic integrated circuits in a compact chip. For the same reason, it can be explained that losses of air-bridge-type PC slab waveguides are as high as 120 dB/mm when operating above the light line [1].

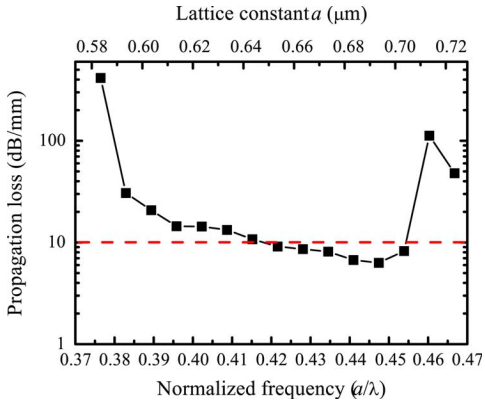

Fig. 6. Transmission spectrum for the ARROW-based PC waveguide. The ARROW-based PC waveguides display propagation losses less than 10 dB/mm in the range of the lattice constant a from 0.651 to 0.704 μm, in which the lowest loss is 6.31 dB/mm ($a = 0.694$ μm).

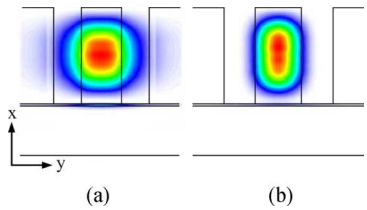

Fig. 7. Power distributions at the frequency of (a) 0.382 and (b) 0.447 (a/λ) in the cross section of the ARROW-based PC waveguide. The corresponding lattice constants are 0.594 and 0.694 μm, respectively.

IV. Bend Losses in Arrow-Based PC Waveguides

For building up compact optical circuits, not only straight waveguides but also bends are required. One of the most attractive features for PC waveguides is to allow sharp bends with low losses. However, the spectral dependence of the bend losses and the propagation losses should be considered at the same time. Some designs of sharp bends focus on achieving high transmission through the corners of the bends, but the spectral range of the high transmission is located above the light line, suffering from severe out-of-plane losses for the PC slab waveguides of high-index-contrast type. As shown in Fig. 3(b), the conventional 60° bend exhibits high transmission in the frequency range where the straight waveguide has high losses. We adopt the same design structure of a 60° bend in [9] and use the similar fashion to design a 120° bend for obtaining high transmission in the frequency range of 0.420 to 0.450 (a/λ), in which the ARROW-based PC waveguide has low propagation losses. For the designed 60° bend, air holes A and B around the corner of the bend are linked by a rectangular air defect with a width equal to the diameter of the air holes and a length of $\sqrt{3}a$, which is the distance between the centers of the holes A and B as shown in Fig. 8(a). The linked hole defect is merged with the air hole C which is located on the site of the triangular lattice in the conventional 60° bend to form the reshaped defect. As shown in Fig. 8(b), the air hole D with a radius $0.35a$ is inserted on the site of the lattice, and an identical linked hole defect except a longer length $2a$ is incorporated in a distance of $0.5a$ to the hole D in the structure of the designed 120° bend. The designed 60° and 120° bends are connected with two single-line defects with

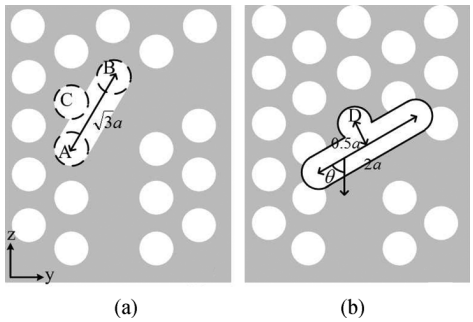

Fig. 8. Schematic pictures of (a) designed 60° and (b) 120° bends. Air holes A, B, and C are located on the sites of the triangular lattice in the conventional 60° bend. For the designed 120° bend, the air hole defect surrounded with a solid line is additionally placed in the structure of the conventional 120° bend. θ is the tilt angle of the linked hole defect with respect to the z-axis and set as 60° in our design.

length of $8a$ along the $\Gamma - K$ direction before and after bends. The bend losses in PC waveguides are mainly due to the large reflections around the corners of the bends, in which periodicity of the lattice is discontinuous. In addition, lightwaves propagating through sharp bends would cause redistribution of the energy and excite the higher order modes, but only the modes matching the guided modes in the output single-line defect can propagate efficiently. The coupling mismatch between the modes at the bends and in the straight waveguides also leads to considerable losses.

To obtain the transmission property of bending waveguides based on the ARROW structure, the approximation in [22] and [23] is adopted at the bends. In this approximation, the air holes on the inner and outer sides of the bend are all assumed as homogeneous air claddings, so the bend region is taken as a short ridge waveguide, in which the confinement of light is support by total internal reflection in the lateral plane and by antiresonance reflection in the vertical direction. The width of the ridge waveguide is $0.916a$, an average width of the bend region. The bend loss would be low when the guided mode in the straight waveguide and the transient mode at the bend region are matched. The propagation constants of the transient mode are calculated by the transfer matrix method and the effective index method. The dispersion curves of the guided mode in the ARROW-based straight PC waveguide and the transient mode at the bend are both shown in Fig. 9(a). For simplicity, the 1-D scattering model [22] is used to estimate the reflection coefficient R through the bend, which is given as

$$R = \left[1 + \left(\frac{2k_g k_t}{[k_g^2 - k_t^2]\sin(k_t L)}\right)^2\right]^{-1} \tag{3}$$

where k_g and k_t are wave vectors of the straight PC and the approximate ridge waveguide, respectively. L is the propagation length of the ridge waveguide, $\sqrt{3}a$ for the 60° bend and $2a$ for the 120° bend, respectively. By this model, only the component of wave vectors along the $\Gamma - K$ direction is considered, and high transmission through the bends can be obtained in the frequency range where k_g and k_t are close. To verify the validity of this model, the 3-D FDTD simulation is performed at the operating wavelength $= 1.55$ μm as shown in Fig. 9(b).

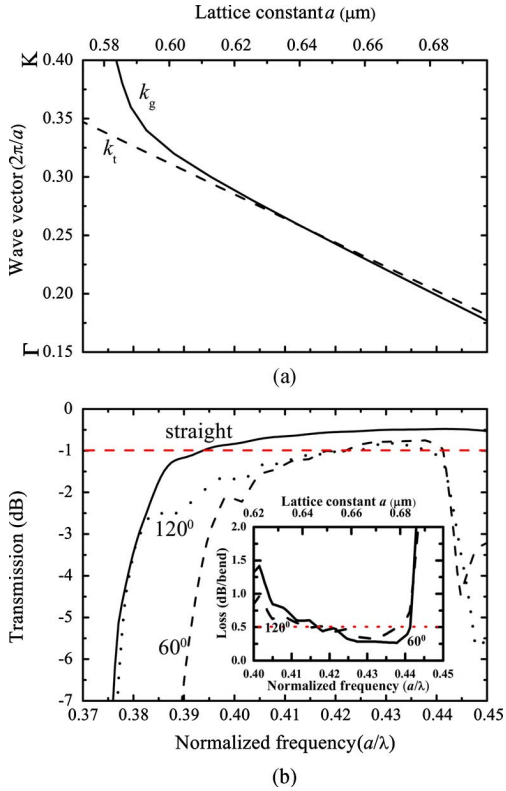

Fig. 9. (a) Dispersion curves of the guided mode (k_g) in the straight PC waveguide and the transient mode (k_t) at the designed bends. (b) Transmission spectra of the 60°, 120° bending and straight PC waveguides based on the ARROW structure. The inset shows the bend loss spectra of the designed bends, in which low loss region (≤ 0.5 dB/bend) is from frequency 0.425 to 0.437 (a/λ). The corresponding lattice constant a is from 0.659 to 0.677 μm.

In order to extract the bend losses, transmission spectra of a straight waveguide with the same propagation length is shown together with that of 60° and 120° bending waveguides. According to the distribution of the dispersion curves, the highest transmission is at the frequency about 0.415 (a/λ) where these two curves cross, but it shifts to 0.438 (a/λ) for the 60° bending waveguide and 0.432 (a/λ) for the 120° one in the 3-D FDTD simulation. This stems from the discrepancy between the 2-D approximation and the 3-D calculation. For the 60° bend, the low bend loss range (transmission ≥ -1 dB) is shown in the frequency range of 0.422 to 0.441 (a/λ). On the other hand, the 120° bend exhibits a lower transmission in the same frequency range because the scattering loss is increased around the corner of the bend. Below the frequency of 0.410 (a/λ), the difference between k_g and k_t becomes large, resulting in invalidity of the 1-D scattering model. It is noticeable that the frequency range of high transmission for the bends agrees with that for the straight waveguide. The bend losses are obtained by normalizing the transmission spectra of bends to that of the straight waveguide as shown in the inset of Fig. 9. For example, bend losses are 0.23 and 0.39 dB/bend at the frequency of 0.435 $(a/\lambda)(a = 0.674\ \mu\text{m})$ for the 60° and 120° bends, respectively. At the same frequency, the propagation loss for the straight waveguide is around 8 dB/mm. As a result, PC waveguides based on the ARROW structure can provide low loss propagation for both straight and bending waveguides in the same frequency range.

V. Conclusion

In summary, the ARROW-based PC waveguide has been proposed and designed. The optical confinement of this device is supported by the photonic band gap in the lateral plane and by the antiresonance reflection in the vertical direction. To obtain a highest transmission efficiency, the depth of PC air holes must be equal to or larger than the thickness of the core layer. In comparison with a conventional PC slab waveguide, the ARROW-based PC waveguide can has flexible design rules with a large core size for improving coupling efficiency with a single-mode fiber to 80.3%. For our designed device operating at a wavelength of 1.55 μm, the propagation losses less than 10 dB/mm can be obtained in the range of the lattice constant from 0.651 to 0.704 μm with the hole radius-to-lattice constant ratio of 0.35. As the designed sharp bends incorporate into the ARROW-based PC waveguide, the normalized frequency range of high transmission for the bends agrees with that for the straight waveguide. For the lattice constant of 0.674 μm, the bend losses are as low as 0.23 and 0.39 dB/bend for the 60° and 120° bends, respectively.

References

[1] M. Notomi, K. Yamada, A. Shinya, J. Takahashi, C. Takahashi, and I. Yokohama, "Extremely large group-velocity dispersion of line-defect waveguides in photonic slabs," *Phys. Rev. Lett.*, vol. 87, no. 25, pp. 253902-1–253902-2, Dec. 2001.

[2] S. J. McNab, N. Moll, and Y. A. Vlasov, "Ultra-low loss photonic integrated circuit with membrane-type photonic crystal waveguides," *Opt. Express*, vol. 11, no. 22, pp. 2927–2939, Nov. 2003.

[3] M. Settle, M. Salib, A. Michaeli, and T. F. Krauss, "Low loss silicon on insulator photonic crystal waveguides made by 193 nm optical lithography," *Opt. Express*, vol. 14, no. 6, pp. 2440–2445, Mar. 2006.

[4] M. V. Kotlyar, T. Karle, M. D. Settle, L. O'Faolain, and T. F. Krauss, "Low-loss photonic crystal defect waveguides in InP," *Appl. Phys. Lett.*, vol. 84, no. 18, pp. 3588–3590, May 2004.

[5] J. Zimmermann, H. Scherer, M. Kamp, S. Deubert, J. P. Reithmaier, A. Forchel, R. März, and S. Anand, "Photonic crystal waveguides with propagation losses in the 1 dB/mm range," *J. Vac. Sci. Technol. B*, vol. 22, no. 6, pp. 3356–3358, Nov./Dec. 2004.

[6] A. Chutinan and S. Noda, "Waveguides and waveguide bends in two-dimensional photonic crystal slabs," *Phys. Rev. B*, vol. 62, no. 7, pp. 4488–4492, Aug. 2000.

[7] M. Qiu, "Effective index method for heterostructure-slab-waveguide-based two-dimensional photonic crystals," *Appl. Phys. Lett.*, vol. 81, no. 7, pp. 1163–1165, Aug. 2002.

[8] A. Chutinan, M. Okano, and S. Noda, "Wider bandwidth with high transmission through waveguide bends in two-dimensional photonic crystal slabs," *Appl. Phys. Lett.*, vol. 80, no. 10, pp. 1698–1700, Mar. 2002.

[9] B. Miao, C. Chen, S. Shi, J. Murakowski, and D. W. Prather, "High-efficiency broad-band transmission through a double-60° bend in a planar photonic crystal single-line defect waveguide," *IEEE Photon. Technol. Lett.*, vol. 16, no. 11, pp. 2469–2471, Nov. 2004.

[10] L. H. Frandsen, A. Harpøth, P. I. Borel, and M. Kristensen, "Broadband photonic crystal waveguide 60° bend obtained utilizing topoloy optimization," *Opt. Express*, vol. 12, no. 24, pp. 5916–5921, Nov. 2004.

[11] P. I. Borel, A. Harpoth, L. H. Frandsen, M. Kristensen, P. Shi, J. S. Jensen, and O. Sigmund, "Topology optimization and fabrication of photonic crystal structures," *Opt. Express*, vol. 12, no. 9, pp. 1996–2001, May 2004.

[12] S. Fasquel, X. Mélique, O. Vanbésien, and D. Lippens, "Three-dimensional calculation of propagation losses in photonic crystal waveguides," *Opt. Commun.*, vol. 246, pp. 91–96, Feb. 2005.

[13] T. D. Happ, M. Kamp, and A. Forchel, "Photonic crystal tapers for ultracompact mode conversion," *Opt. Lett.*, vol. 26, no. 14, pp. 1102–1104, Jul. 2001.

[14] D. W. Prather, J. Murakowski, S. Shi, S. Venkataraman, A. Sharkawy, C. Chen, and D. Pustai, "High-efficiency coupling structure for a single-line-defect photonic-crystal waveguide," *Opt. Lett.*, vol. 27, no. 18, pp. 1601–1603, Sep. 2002.

[15] P. E. Barclay, K. Srinivasan, M. Borselli, and O. Painter, "Probing the dispersive and spatial properties of photonic crystal waveguides via highly efficient coupling from fiber tapers," *Opt. Lett.*, vol. 85, no. 1, pp. 4–6, Jul. 2004.

[16] M. A. Duguay, Y. Kokubun, T. L. Koch, and L. Pfeiffer, "Antiresonant reflecting optical waveguides in SiO2-Si mutilayer structures," *Appl. Phys. Lett.*, vol. 49, no. 1, pp. 13–15, Jul. 1986.

[17] T. Baba and Y. Kokubun, "Dispersion and radiation loss charateristics of antiresonant reflecting optical waveguides-numerical results and analytical expressions," *IEEE J. Quantum Electron.*, vol. 28, no. 7, pp. 1689–1790, Jul. 1992.

[18] T. Zijlstra, E. van der Drifta, M. J. A. de Dood, E. Snoeks, and A. Polman, "Fabrication of two-dimensional photonic crystal waveguides for 1.5 μm in silicon by deep anisotropic dry etching," *J. Vac. Sci. Technol. B*, vol. 17, no. 6, pp. 2734–2739, Nov./Dec. 1999.

[19] S. W. Leonard, H. M. van Driel, A. Birner, U. Gösele, and P. R. Villeneuve, "Single-mode transmission in two-dimensional macroporous silicon photonic crystal waveguides," *Opt. Lett.*, vol. 25, no. 20, pp. 1550–1552, Oct. 2000.

[20] C. Sauvan, P. Lalanne, J. C. Rodier, J. P. Hugonin, and A. Talneau, "Accurate modeling of line-defect photonic crystal waveguides," *IEEE Photon. Technol. Lett.*, vol. 15, no. 9, pp. 1243–1245, Sep. 2003.

[21] A. Morand, C. Robinson, Y. Désières, T. Benyattou, P. Benech, O. Jacquin, and M. Le Vassor d'Yerville, "3-D numerical modeling of propagation losses of a single line-defect photonic crystal," *Opt. Commum.*, vol. 221, pp. 353–357, Jun. 2003.

[22] A. Mekis, J. C. Chen, I. Kurland, S. Fan, P. R. Villeneuve, and J. D. Joannopoulos, "High transmission through sharp bends in the photonic crystal waveguides," *Phys. Rev. Lett.*, vol. 77, no. 18, pp. 3787–3790, Oct. 1996.

[23] Y. Zhang and B. Li, "Ultracompact waveguide bends with simple toplogy in two-dimensional photonic crystal slabs for optical communication wavelengths," *Opt. Lett.*, vol. 32, no. 7, pp. 787–789, Apr. 2007.

Yu-Lin Yang was born in Taipei, Taiwan, in 1980. He received the B.S. degree in physics from National Central University, Jhongli, Taiwan, in 2002 and the M.S. degree in electronics from National Chiao Tung University, Hsinchu, Taiwan, in 2004. He is currently working toward the Ph.D. degree in electronics at National Chiao Tung University.

His current research is focused on 2-D photonic crystal waveguides and optical properties of 3-D metallic photonic crystals.

Shih-Hsin Hsu (S'99–M'06) received the B.S. degree in physics from the National Taiwan University, Taipei, Taiwan, in 1994 and the Ph.D. degree in electronics from the National Chiao Tung University, Hsinchu, Taiwan, in 2005.

He is a Postdoctoral Research Fellow with the Research Center for Applied Sciences, Academia Sinica, Taipei. His current research is focused on nanophotonics and optical characterizations.

Ming-Feng Lu was born in Taiwan, in 1963. He received the B.S. degree in electrical engineering from National Cheng Kung University, Tainan, Taiwan, in 1985 and the M.S. degree in electronics from National Chiao Tung University, Hsinchu, Taiwan, in 1990. He is currently working towards the Ph.D. degree in electronics at National Chiao Tung University.

He is an Associate Professor in the Department of Electronics Engineering, Minghsin University of Science and Technology, Hsinfeng, Hsinchu, Taiwan. He has focused his research on photonic crystal devices for integrated optics and optical communication applications.

Yang-Tung Huang (M'90) was born in Taiwan, in 1955. He received the B.S. degree in electrophysics and the M.S. degree in electronics from National Chiao Tung University, in 1978 and 1982, respectively, and the Ph.D. degree in electrical and computer engineering (minor in optical sciences) from the University of Arizona, Tucson, in 1990.

He is a Professor in the Department of Electronics Engineering and the Institute of Electronics, and a Joint Professor at the Department of Biological Science and Technology, National Chiao Tung University. He has been the Director of the Institute of Electronics for three years, the Director of Semiconductor Research Center for two years, and the Director of Nano Facility Center for four years. His current researches include integrated optics, photonic crystal waveguides, bio-optoelectronics, and optoelectronic switching networks.

Prof. Huang received the Outstanding Research Award from the National Science Council in 1998.